ELSEVIER

Surface Science 389 (1997) 338–348

surface science

Comparison of reflection high-energy electron diffraction and low-energy electron diffraction using high-resolution instrumentation

Bert Müller [a,b,*], Martin Henzler [a]

[a] *Institut für Festkörperphysik, Universität Hannover, Appelstr. 2, D-30167 Hannover, Germany*
[b] *Institut für Quantenelektronik, Eidgenössische Technische Hochschule Zürich, CH-8093 Zürich, Switzerland*

Received 15 March 1997; accepted for publication 9 June 1997

Abstract

Reflection high-energy electron diffraction (RHEED) is a standard diffraction method in surface science, but contrary to low-energy electron diffraction (LEED) the analysis of morphology and defect structure is not as reliable due to inelastic scattering and a more complicated scattering geometry. These difficulties are mastered by adequate instrumentation and measuring procedures as done with a novel high-resolution, energy-filtered RHEED instrument. The elastically scattered intensity close to the specular beam is measured for many angles of incidence in both directions – parallel and perpendicular to the shadow edge. The series of profiles obtained perpendicular to the shadow edge have been used to produce profiles with constant momentum transfer perpendicular to the surface corresponding to LEED profiles with ultra-high resolution. By means of these profiles, the surface morphology is characterized on the basis of kinematic approximation as done in LEED with much success. The validity of that procedure is demonstrated for homoepitaxy on Si(111) by comparison of the results with LEED and STM data. © 1997 Elsevier Science B.V.

Keywords: Epitaxy; Low energy electron diffraction; Low index single crystal surfaces; Molecular beam epitaxy; Reflection high-energy electron diffraction; Silicon; Surface defects

1. Introduction

Electron diffraction techniques (RHEED and LEED) have been used to characterize the crystalline structure of surfaces, since electrons have been the strong-scattering probes of choice for the study of crystals at atomic distance scales with extremely high surface sensitivity. The essential advantage of RHEED in relation to other surface sensitive techniques is that RHEED does not need much space around the sample and the normal incidence is free for any treatment, e.g. deposition. Therefore, RHEED has become the standard tool in molecular beam epitaxy (MBE) for in situ characterization, especially during epitaxial growth. In principle, RHEED and LEED yield the same information about all periodicities in space and time of the static and growing surface, i.e. the lattice constants, the surface reconstructions, the position of the atoms within the unit cell by the analysis of rocking curves and I/V curves, respectively, the growth modes and the growth velocity by intensity oscillations as well as the defect structure of the surface. These parameters represent exact mean values of the area illuminated by the electron beam. A detailed quantitative study of the surface morphology by RHEED, however,

* Corresponding author. Fax: (+41) 1 633.1056; e-mail: bert.mueller@iqe.phys.ethz.ch

PII S0039-6028(97)00447-0

is more or less complicated since dynamic effects and inelastic scattering play an important role. Therefore, RHEED has not been used in the same way as LEED to quantify surface morphology and surface defects from spot profiles using the kinematic approximation [1–3].

The purpose of this paper is to compare RHEED and LEED on the basis of experimental results obtained by a high-resolution RHEED system [4]. First of all energy filtering removes all losses $\Delta E > 4$ eV, so that spot broadening by plasmon losses is avoided. The refraction of electrons at the vacuum–crystal interface is treated quantitatively, so that surface and bulk effects are separated. Using the well-developed procedures of spot profile analysis in LEED, RHEED profiles are evaluated after converting them into the LEED geometry. A comparison with LEED and STM results proves the validity of the procedures. In this way the grazing incidence of the electron beam in RHEED is used for a quantitative analysis of surface morphology with extremely high resolution.

The kinematic approximation is used with different techniques (for a comparison see e.g. Ref. [5]). It works without any restriction for X-ray scattering [6,7]. A synchrotron radiation source (preferentially with a wiggler or undulator) compensates for low surface sensitivity. For fast measurements and not so perfect samples, electron diffraction has the advantage of high surface sensitivity. Here however, the validity of the approximation has to be checked. For LEED, it has been approved not for the integral intensity, rather for profiles after normalization with the integral intensity. The discussion will demonstrate that it works in the same way for RHEED, when the profiles are taken with $K_\perp = \text{constant}$.

2. Experimental

The RHEED measurements were carried out with a high-resolution system (SPA-RHEED) described elsewhere [4]. The Si sample of size 7 mm × 22 mm, precisely oriented into the (111) direction (within 0.044°), was heated by direct current up to about 1200°C to remove the oxide and some of the outermost layers. This procedure results in a perfect (7 × 7)-reconstructed surface with large terraces. In order to produce different morphologies, about 10 bilayers (BL) of Si were deposited onto such a well-prepared surface by a water-cooled e-beam evaporator. The growth rate of 0.3 bilayers per minute (BL min^{-1}) was determined by the RHEED intensity oscillations. The temperature of the sample was measured by an infrared pyrometer. The background pressure was always well below 2×10^{-10} mbar.

The primary energy of the electron beam (4–10 keV, stabilized to less than 1 eV) was measured with a precision resistive voltage divider (precision better than 3 eV).

The absolute and relative angles have been determined in different ways. The position of the shadow edge is a rough estimate. Also, the measurement of the relative angles of the Laue circles provides only a limited accuracy. As already shown by other groups [8,9], the best way to determine the angle of incidence is the measurement of the angle between the primary and specular beam (accuracy about 1 mrad). Any angle of incidence is reproduced and accurately varied with a laser beam reflected from the sample (accuracy < 0.1 mrad).

At the exact in-phase condition (Bragg angle), the specular beam is indeed perfectly round and not elongated [10]. Changing the angle of incidence by 2 mrad, the spot becomes clearly elongated. This observation is used to verify the absolute values of the angles of incidence, since the round spot is due to a scattering vector equal to a vector of the reciprocal lattice (here, e.g. (111) or (222)).

All profiles shown in this paper are energy filtered. By adjusting the retarding field in front of the detector, all electrons with losses higher than 4.5 eV are suppressed.

3. Conversion of RHEED profiles into a reciprocal lattice rod

The reciprocal lattice and the Ewald construction are very powerful tools to describe electron diffraction phenomena. Fig. 1 shows the Ewald construction for nearly normal incidence and low primary energy (LEED) as well as for grazing

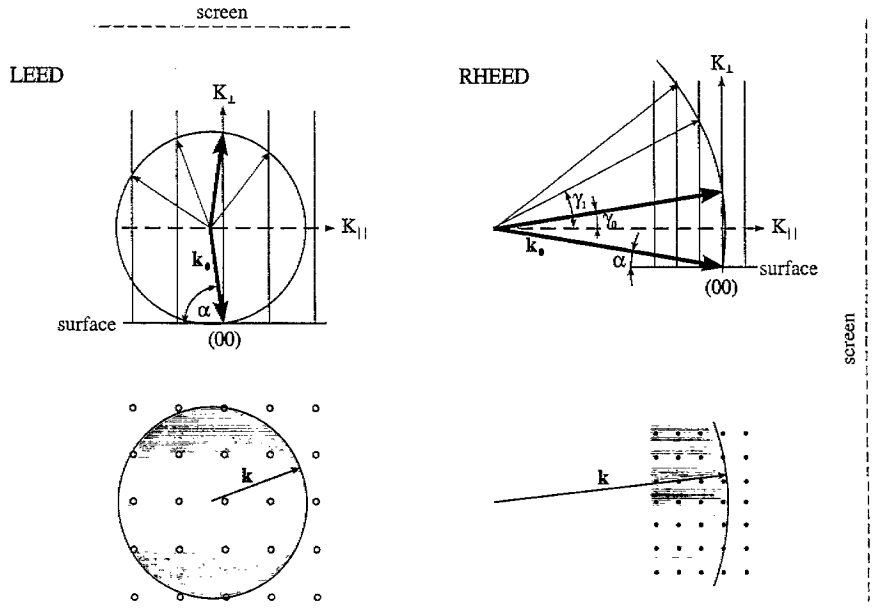

Fig. 1. The Ewald construction for an ideal surface in LEED and RHEED geometry. The indicated "screen" shows the plane onto which the Ewald sphere is projected.

incidence and high primary energy (RHEED) applied to an ideal two-dimensional surface. The crossing points of the Ewald sphere with the rods of the reciprocal lattice define the directions of the diffracted beams detected by a screen (or a channeltron). The specular beam – the (00) spot – already contains most of the morphologic information, such as terrace widths, but not, however, the lateral lattice constant. Therefore, the quantitative analysis is at first restricted here to evaluation of data around the specular beam.

In LEED, the Ewald sphere cuts the (00) rod almost orthogonally while in RHEED the Ewald sphere cuts the (00) rod by a small angle. The spot profiles in LEED are usually evaluated from cross sections through the reciprocal lattice rod with $K_\perp$ = constant. On the other hand, a single profile in RHEED (within the plane of incidence) includes mainly variations in $K_\perp$ while the variations of $K_\parallel$ are small. In LEED as well as in RHEED there are drastic changes in the intensity if $K_\perp$ is varied. Therefore, the RHEED profiles should be converted to a cross section where $K_\perp$ is constant, both to avoid complications from dynamic scattering and to compare them easily with LEED profiles. The aim of this procedure is the application of spot profile analysis on the basis of kinematic approximation to quantify the surface morphology making use of the advantages of RHEED.

When the RHEED profile is taken normal to the plane of incidence, $K_\perp$ is already almost constant. Therefore, the profile is directly comparable with LEED data, especially since the transfer width of the used RHEED instrument in this direction equals that of high-resolution SPA-LEED systems (about 200 nm) [4,11].

For profiles within the plane of incidence, the transfer width is increased by a factor of $1/\sin\alpha$ (α is the angle of incidence) due to the reduced variation of $K_\parallel$ in a scan [12]. To convert such profiles into those with $K_\perp$ = constant, many profiles have been recorded for the same primary energy and different angles of incidence with 500 to 2000 points each (cf. Fig. 2).

Since the primary energy and, therefore, the wave vector k_0, the angle of incidence α and the deflection angles γ are known, the perpendicular and parallel components of the scattering vector – $K_\perp$ and $K_\parallel$ – are given, as fractions of the vectors

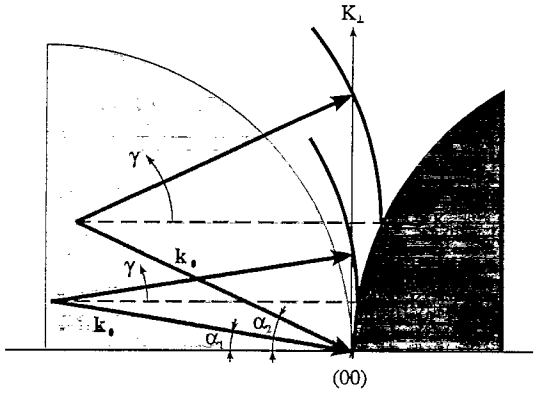

Fig. 2. The construction of a reciprocal lattice rod by RHEED profiles within the plane of incidence. The gray colored region on the left is not accessible since the angle of incidence α has to be larger than zero. The region between the direct beam and shadow edge is also not accessible (dark colored), since the angle γ has to be larger than zero.

of the 3D reciprocal lattice.

$$K_\perp = \frac{d_\perp}{2\pi} k_0(\sin\gamma + \sin\alpha), \quad (1)$$

$$K_\parallel = \frac{d_\parallel}{2\pi} k_0(\cos\gamma - \cos\alpha). \quad (2)$$

$d_\perp$ and $d_\parallel$ correspond to the lattice plane distances perpendicular to the surface and parallel to the surface *in the scattering plane* ($d_\perp = d_{111}$; $d_\parallel = d_{110}$ or $d_\parallel = d_{112}$ depending on the azimuth). The scattering vectors, defined here as relative values, are given in units of "%BZ" – per cent Brillouin zone. Two portions of the reciprocal space cannot be detected since both the angle of incidence α and of exiting γ have to be larger than zero (gray colored in Fig. 2).

By interpolation of more than 100 RHEED profiles each containing 500 points obtained perpendicular to the shadow edge through the specular beam (i.e. the direction of high resolution) we have constructed a reciprocal lattice rod of the well prepared Si(111) surface heated to 1200°C which is presented in Fig. 3. The measuring time for obtaining a profile was about 30 s. Attention should be paid to the different scales of $K_\parallel$ and $K_\perp$. $K_\parallel$ covers ±5%BZ while $K_\perp$ covers more than

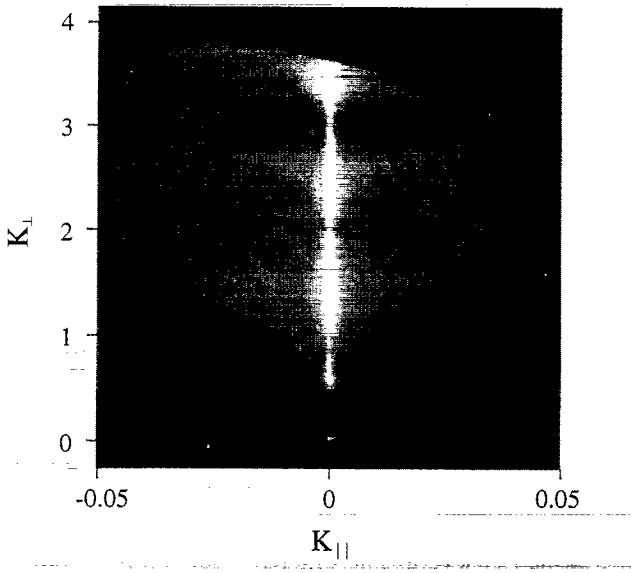

Fig. 3. A reciprocal lattice rod constructed by high-resolution, energy-filtered RHEED profiles running perpendicular to the shadow edge for the Si(111)-7×7 reconstructed surface at a primary electron energy of 6124 eV. The direction of incidence was rotated by 4.4° out of the [0$\bar{1}$1] azimuth. All electrons with energy losses of more than 4.5 eV were suppressed. Note, $K_\parallel$ and $K_\perp$ are differently scaled. Because $K_\perp/K_\parallel$ is almost 50, the scans and the shadow edge are strongly distorted.

400%BZ. A part of the direct beam is clearly seen at $K_\perp = 0$; $K_\parallel = 0$.

The shadow edge is a typical feature of a RHEED pattern. It is clearly visible due to the high amount of plasmon scattered electrons, which can be increased to more than 99.9% near to the shadow edge [10]. The electrons, inelastically scattered by surface and bulk plasmons are suppressed by our energy filter. Therefore, the shadow edge is not seen any more in our energy-filtered 2D scans. In the high-resolution profiles, however, we are able to detect some elastic intensity due to the higher dynamic range. Thus, the shadow edges of the different profiles are also present in the special representation of the reciprocal lattice rods as shown in Fig. 3 (cf. also scheme of Fig. 2).

The reciprocal lattice rod possesses nodes. These nodes are equidistant and appear when the electrons interfere constructively at the biatomic steps of the surface, which corresponds to a multiple integer of $K_\perp$ and, therefore, the in-phase condition for scattering from neighboring terraces.

At these in-phase conditions, the intensity is expected to have a maximum, as shown e.g. in Fig. 6. In Fig. 3, however, one finds only a relative maximum at $K_\perp = 2$ and $K_\perp = 3$, and at $K_\perp = 1$, there is not even an intensity maximum. The occurrence of well-pronounced intensity maxima strongly depends on the particular scattering conditions. This experimental observation supports the above statement that one should only consider relative intensities in a profile with $K_\parallel$ = constant for a quantitative evaluation, since the rocking curves may be dominated by dynamic effects. The full-width-at-half-maximum (FWHM) of the profiles at the different in-phase conditions is given by the resolution of the diffractometer if mosaic broadening can be neglected. The inverse of the half-width provides the system transfer width, which is several micrometers wide. Samples show usually smaller average terrace sizes, so the whole range of terrace widths up to about 5 μm can be investigated by SPA-RHEED. In Fig. 3, it is seen that the FWHM of the nodes increases with increasing $K_\perp$ due to the larger angles of incidence.

The lattice rod is symmetric with respect to $K_\parallel$. This seems to be surprising, since the intensity at the right- and left-hand side are obtained at different angles of incidence. The fact that the intensity can change by orders of magnitude, even for small variations of the angle of incidence, is well known from rocking curves [13]. A second thought, however, shows that the lattice rod has to be symmetric for special conditions. When in Eqs. (1) and (2) the angle of incidence α and the angle of detection γ are exchanged, the normal component of the scattering vector $K_\perp$ is conserved and the parallel component $K_\parallel$ changes its sign. For a surface with two-fold rotational or mirror symmetry the scattering condition is, therefore, identical, when only the sign of $K_\parallel$ is reversed. The Si(111) surface has a three-fold symmetry and mirror planes. When the plane of incidence is normal to a mirror plane, this symmetry is given. For the other symmetric azimuths, the two-fold symmetry is nearly fulfilled due to the six-fold symmetry of the single (111) plane. Moreover, our experiments demonstrate that also for significant changes from a symmetric azimuth (e.g. see Fig. 3: 4.4°), one obtains highly symmetric lattice rods. This experimental result is comparable with LEED results where dynamic effects are negligible within the range of broadening due to disorder at the surface. Inelastically scattered electrons only lead to a broadening of the rod, whereby multiple scattering does not affect this symmetry of the rod.

The nodes of the lattice rod are equidistant due to constructive interference at the biatomic surface steps. If the interference is due to the diffraction from deeper layers, the electrons are first refracted at the crystal–vacuum interface giving rise to a considerable change of the nodes position, as shown in detail in Appendix A. Since the position of the nodes reflects the surface interference, the lattice rods may be used to analyze the surface morphology. The intensity, however, is determined by multiple scattering including deeper layers. This effect is especially clear for a high symmetry azimuth (considerable variation of intensity in Fig. 4) where the surface resonances are essentially increased. Therefore, one should avoid these scattering conditions for quantitative profile analysis.

4. Profile analysis from reciprocal lattice rods

The validity of the proposed procedures is verified for the homoepitaxial growth on Si(111). On

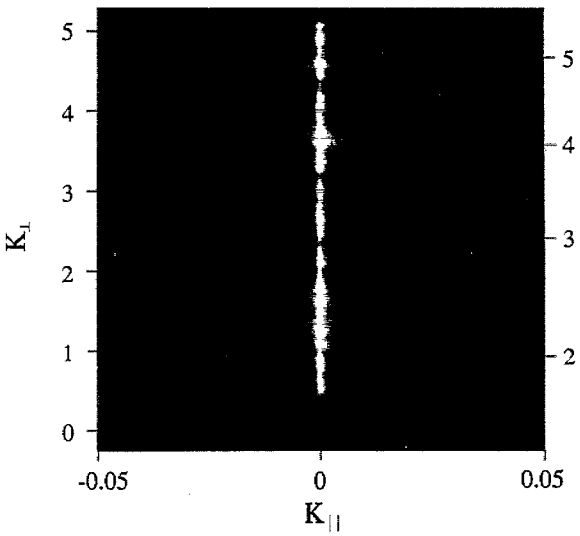

Fig. 4. A reciprocal lattice rod of Si(111)-7 × 7 with the incident beam in the symmetric azimuth at a primary electron energy of 6121 eV.

the one hand, many experimental studies have been carried out, and high-resolution LEED [14] and STM data [15,16] are available for quantitative comparison. On the other hand, large terraces can be produced to prove the ultra-high resolution of RHEED. The analysis has been started from a well annealed Si(111) surface. Onto that surface about 10 BL silicon was deposited at a fixed deposition rate (0.3 BL min^{-1}) at different substrate temperatures (480, 530 and 580°C) to realize different surface morphologies. In agreement with the LEED and STM experiments, the samples prepared at 1200 and 580°C are only (7×7) reconstructed while at the lower substrate temperatures one obtains a mixture of (5×5) and (7×7) reconstruction as seen in Fig. 5.

For all of these samples, reciprocal lattice rods have been generated. These rods always show for a cross section with constant $K_\perp$ a highly symmetric shape. This symmetry is demonstrated for a typical set of profiles in Fig. 6 for the sample grown at 580°C. These profiles with $K_\perp$=constant correspond astonishingly to those of high-resolution LEED profiles [14], so that the evaluation is done in the same way. The correspondence is the same for $K_\parallel$ within the plane of incidence or normal to it. So the advantage of higher transfer width for scattering within the plane of incidence may be used here.

The profiles for the out-of-phase condition ($K_\perp=1.5$) are shown in Fig. 7. From these out-of-phase profiles, the average terrace widths are derived [17,18] using the same procedure as in Ref. [14]. The data shown as Arrhenius plot are compared with LEED [14] and STM [15,16] results for a deposition rate of 0.3 BL min^{-1} in Fig. 8. The LEED and STM data are scaled to this deposition rate assuming a critical island size of $i^*=2$ and $i^*=6$, respectively, as given by the different authors, since the critical island size is expected to depend on deposition rate. Although the coverage is much lower for the STM investigation (0.15 BL), the agreement with the RHEED data is excellent. Also the LEED data agrees well with the RHEED results. The deviation at lower substrate temperatures is not clear, but we believe that the low ratio between monomer diffusion constant and deposition rate ($\sim10^3$), a phenome-

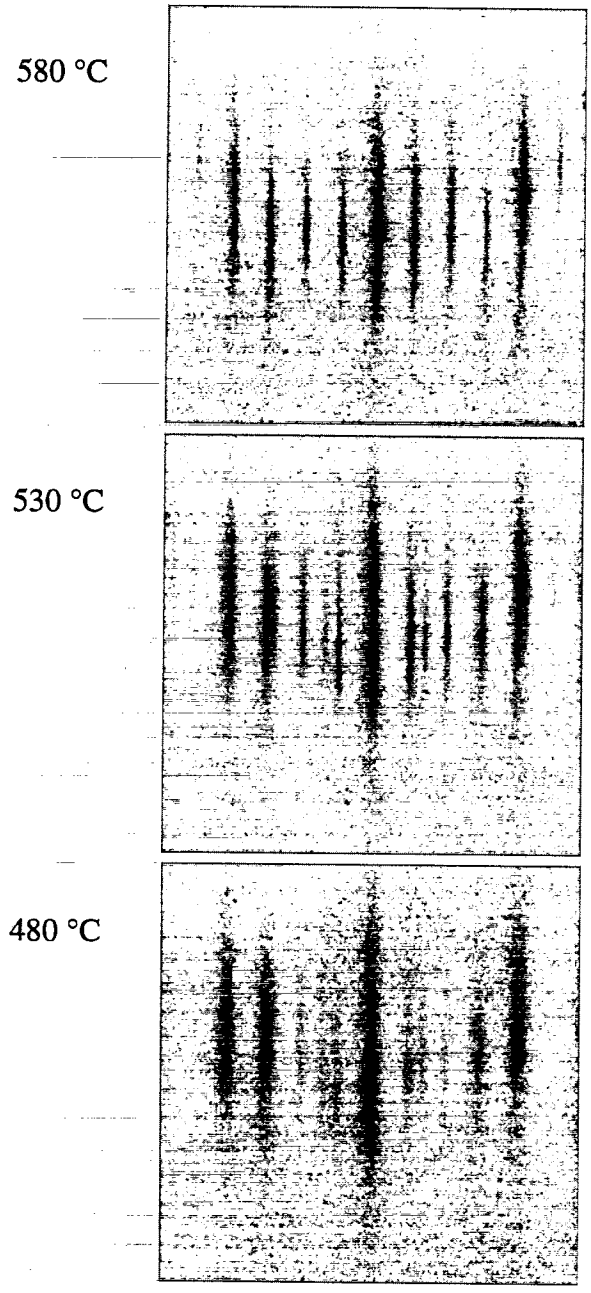

Fig. 5. RHEED pattern of 10 BL Si on Si(111) grown at different substrate temperatures (480, 530 and 580°C) and a fixed deposition rate (0.3 BL min^{-1}) resulting in different surface morphologies ([00$\bar{1}$] azimuth; primary energy: 6130±10 eV; angle of incidence: 2.20±0.05°).

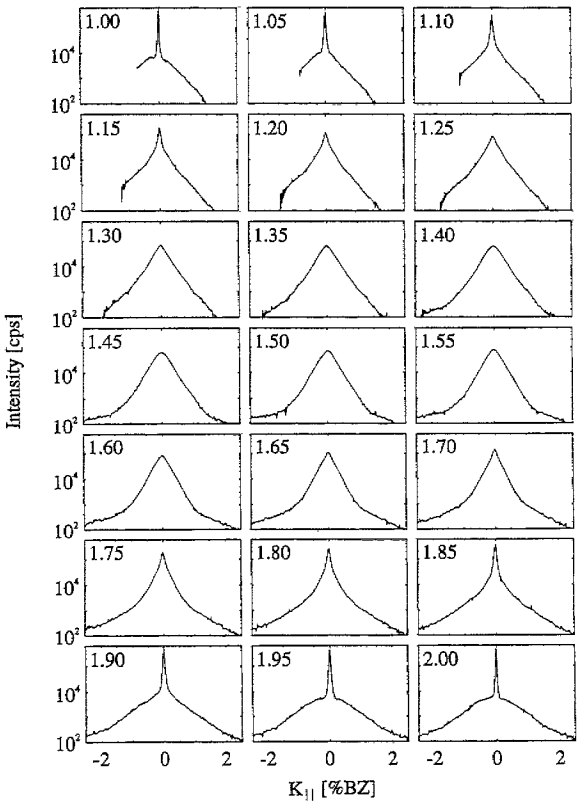

Fig. 6. A series of spot profiles with constant $K_\perp$ within the plane of incidence for the sample grown at 580°C. The profiles are highly symmetric and show the ultra-high resolution and the high dynamic range. The numbers in the upper-left of each profile are the values of the normal component of the relative scattering vector $K_\perp$.

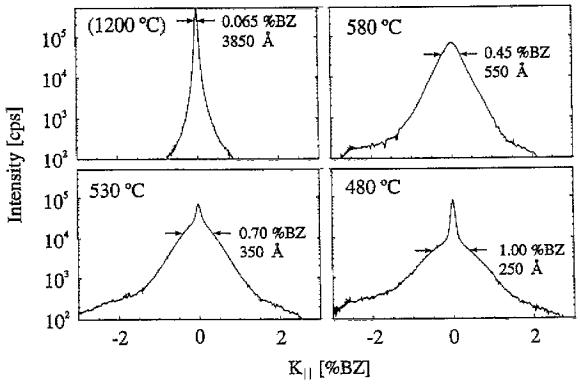

Fig. 7. Profiles as in Fig. 6 at the out-of-phase condition ($K_\perp = 1.5$) for differently prepared surfaces. The arrows indicate the *FWHM* of the shoulder in the profiles and the related mean terrace sizes.

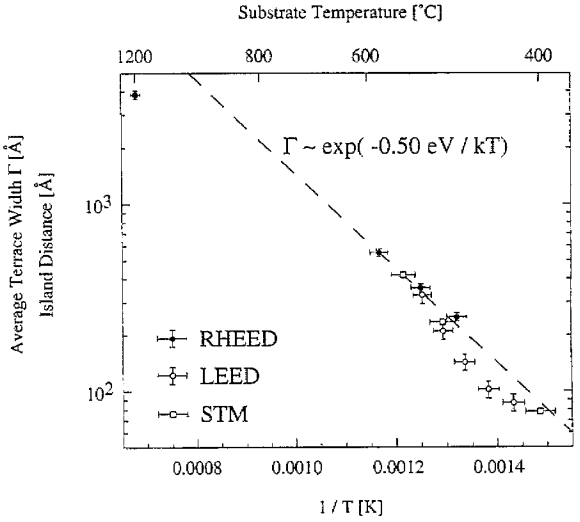

Fig. 8. Arrhenius-plot for the average terrace width and island distance, respectively, for homoepitaxy on Si(111) to compare RHEED, LEED and STM results. The result at 1200°C is shown to demonstrate the extremely high resolution of RHEED and the suitable preparation of the substrate.

non which leads to post-deposition effects [19], is responsible for the deviation. This may be also the reason that the authors found a smaller size for the critical nucleus. The rate dependent change of the size of the critical nucleus was already found by REM studies for Si/Si(111) [20]. This study delivers slightly higher values for the average terrace width with rather large error bars.

For in-phase condition (integer values for $K_\perp$) the kinematic approximation predicts for a stepped surface (with no other defects) a sharp profile as given by the instrument without any shoulder. Figs. 9 and 10 show, that the central spike (as given by the instrument) dominates the profile, a shoulder with a peak intensity of about 1%, however, is visible. Often, this shoulder has a ring-like shape. The half-width of the shoulder is independent of phase (Fig. 9) and about twice that of the profile for the out-of-phase condition (Figs. 7 and 10). It is therefore well described within the kinematic approximation by a morphological defect with a scattering factor different from that of the periodic superstructure and related to the superstructure domains. This shoulder is also present in LEED profiles at the in-phase condition [21] and

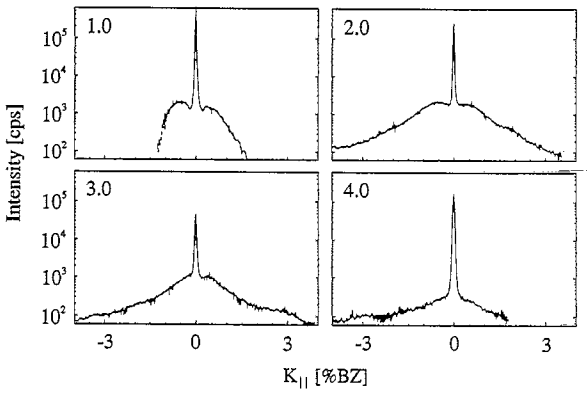

Fig. 9. Profiles as in Fig. 6 for a sample grown at 530°C at the different in-phase conditions. The value of $K_\perp$ is given in the upper-left of each profile.

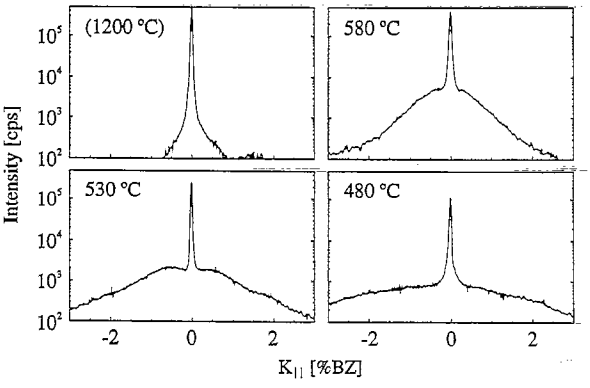

Fig. 10. Profiles as in Fig. 6 at the in-phase condition ($K_\perp = 2$) for the differently prepared samples.

seems to be inherent of DAS-structures. It vanishes after the surface is covered by antimony resulting in a well ordered $(\sqrt{3} \times \sqrt{3})$-reconstruction [21]. Therefore, we conclude that the domain boundaries of the DAS structures have more disorder than the $\sqrt{3}$ structures, so that a substantial fraction of the surface shows a different form factor producing the shoulder also for in-phase condition. For decreasing growth temperatures, the domains become smaller and the fraction of surface atoms in the boundaries becomes higher. Therefore, the central peak does not completely vanish even for the out-of-phase condition at substrate temperatures below ~500°C for both RHEED (cf. Fig. 7) and LEED [14]. These effects become clearer in RHEED than in LEED due to the much higher resolution.

The perfect agreement between RHEED and the other experimental studies for Si/Si(111) shows the validity of the kinematic evaluation of the energy-filtered RHEED profiles with $K_\perp$ = constant. Now, the extended resolution of RHEED can be used in the region beyond SPA-LEED resolution.

5. Comparison of RHEED and LEED

The development of a high-resolution, energy-filtered RHEED instrument which is capable of suppressing plasmon losses permits a morphological analysis of the RHEED data with a precision heretofore unobtainable. The linearity, the dynamic range and the resolution are far superior to those of conventional systems. The simple change of the detected angular range over 3 orders of magnitude or even more by means of the electrostatic double-octupole allows us to construct reciprocal lattice rods and to obtain profiles of ultra-high resolution which are analyzable in the same way as LEED profiles.

Both RHEED and LEED multiple scattering requires a dynamic scattering theory for calculation of the intensities. Those theories are available for both techniques as long as the surface is strictly periodic. For surfaces with steps and other defects no dynamic theories are developed except for an averaged surface after projection along the direction of the incident beam [22,23]. For analysis of the lateral structure in LEED the kinematic approximation has been shown to be valid in many cases. The present RHEED investigation demonstrates, that this approximation can be used in the same way for scans perpendicular to the shadow edge after converting them to scans with $K_\perp$ = constant, as shown for Si homoepitaxy in the preceding section. Here, the resolution is extended to the micrometer region. Hence, LEED and RHEED are comparable techniques with respect to morphological analysis of surfaces, whereby RHEED has essential advantages among others due to the increased resolution and the open

geometry in front of the sample for other treatments.

A new instrumental development – a combination of two double-octupoles, one between gun and sample and one between sample and detector – enables a direct scan with $K_\perp$ = constant without the need to convert many scans. Then RHEED profiles are as easily obtained as LEED profiles.

Acknowledgements

The investigation has been supported by the Volkswagen Stiftung. We gratefully acknowledge the help of D. Jürgens for data conversion and J. Wollschläger for valuable discussions.

Appendix A

6.1. *Refraction of electrons at the vacuum–crystal interface*

The atoms are periodically arranged and the average of the resulting electrostatic potential distribution, over the volume of the crystal, is positive and a few volts in magnitude. This mean potential is called the inner potential. The inner potential of the sample Φ affects the refraction of the incident and the diffracted electron beams, i.e. the beams change their direction of propagation and their magnitude at the vacuum–crystal interface and vice versa. For electron diffraction, it is convenient to consider the wave vectors $\boldsymbol{k}_0$ and $\boldsymbol{q}$ in the vacuum and the crystal, respectively

$$\boldsymbol{k}_0 = \frac{1}{\hbar}\sqrt{2meE}, \tag{A.1}$$

$$\boldsymbol{q} = \frac{1}{\hbar}\sqrt{2me(E+\Phi)}, \tag{A.2}$$

where $\hbar$ is Planck's constant, m the electron mass, e the electron charge and E the primary electron energy. Based on the Maxwell equations, it is evident that the tangential component of the wave vectors have to be conserved at the interface.

$$\boldsymbol{k}_t = \boldsymbol{q}_t. \tag{A.3}$$

Fig. 11 shows the relation between the incident and the refracted beam. One can introduce the refractive index n

$$n = \frac{\cos\alpha}{\cos\beta} = \frac{\boldsymbol{k}_t/\boldsymbol{k}_0}{\boldsymbol{q}_t/\boldsymbol{q}} = \frac{\boldsymbol{q}}{\boldsymbol{k}_0} = \sqrt{\frac{E+\Phi}{E}}. \tag{A.4}$$

The refractive index depends on the primary energy of the electrons and on the inner potential of the sample. In RHEED, the refractive index deviates from one by about 10^{-3}. Although this value is very small, it gives rise to a notable effect as we will show with the example of silicon. The inner potential of silicon is reported as 12 V [24].

The influence of the inner potential on the radius of the Ewald sphere is summarized for different LEED and RHEED energies in Table 1. Contrary to LEED, the radius of the Ewald sphere for electrons penetrating the crystal has not to be corrected for the higher RHEED energies.

Two different scattering conditions may be described as Bragg reflection and Bragg scattering, respectively. For a stepped surface, all terraces scatter in-phase when the perpendicular component of the scattering vector in vacuum coincides with $2\pi/d$, whereby d is the step height. Such an

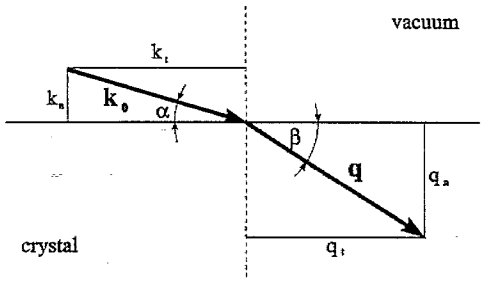

Fig. 11. The refraction of electrons at the vacuum–solid interface.

Table 1
Influence of refraction on the radius of the Ewald sphere using an inner potential of 12 V (silicon)

E (eV)	k_0 (Å^{-1})	q (Å^{-1})	$(q-k_0)/k_0$
10	1.620	2.403	0.48
100	5.123	5.422	0.058
1000	16.202	16.299	0.006
10000	51.235	51.265	0.0006

Table 2
Influence of refraction on Bragg angles using an inner potential of 12 V (silicon)

m	$E=10$ eV		$E=100$ eV		$E=1000$ eV		$E=10000$ eV	
	α_B	δ_B	α_B	δ_B	α_B	δ_B	α_B	δ_B
(111)	38.204	–	11.278	–	3.546	–	1.121	–
(222)	–	35.062	23.026	10.467	7.105	3.293	2.242	1.041
(333)	–	–	35.925	28.265	10.693	8.612	3.364	2.714
(444)	–	–	51.472	44.542	14.323	12.815	4.487	4.022
(555)	–	–	77.927	66.130	18.013	16.809	5.612	5.247

in-phase condition is observed as a sharp spot in SPA-LEED [25] and SPA-RHEED [10]. The angle of incidence for the surface Bragg condition is given by

$$\sin \alpha_B = m \frac{\pi}{dk_0}. \tag{A.5}$$

For Bragg reflections at the planes inside the crystal the wave vector $\boldsymbol{q}$ has to be used, so that the angle of incidence β_B is derived from

$$\sin \beta_B = m \frac{\pi}{dq}, \tag{A.6}$$

where m is the diffraction order (integer), and d is the vertical distance from plane to plane.

Experimentally, this bulk Bragg reflection is observed by the crossing of Kikuchi lines in RHEED geometry. In order to obtain the angle β_B inside the crystal, outside the angle δ_B must be adjusted which is derived from refraction at the surface, using $k_t = q_t$ (tangential components) and $q_n^2 = k_n^2 + 2me\Phi/\hbar^2$ (normal components), so that

$$\cos \delta_B = n \cos \left\{ \arcsin\left(m \frac{\pi}{d} \frac{\hbar}{\sqrt{2meE}} \frac{1}{n} \right) \right\}. \tag{A.7}$$

In Table 2 the Bragg angles α_B and δ_B for different electron energies and different diffraction orders are compared. This comparison reveals the drastic influence of the refraction to the Bragg angles. The (111) reflections inside the crystal cannot be generated for any primary energy and if such a trajectory is formed (e.g. by inelastic scattering or at a certain amount of steps) the electrons cannot leave the crystal. For RHEED energies and grazing incidence, the refraction effect has to be considered for data analysis.

That means, one can use the refraction of electrons at the vacuum–crystal interface to determine the surface sensitivity of RHEED with respect to terrace step structure, since bulk and surface phenomena can be separated. The distances between the nodes of a reciprocal lattice rod are equidistant for surface scattering and become less dense for lower orders in the case of bulk scattering. For silicon, the extremely high surface sensitivity of RHEED with respect to surface morphology is demonstrated in this communication.

References

[1] M. Henzler, in: H. Ibach (Ed.), Electron Spectroscopy for Surface Analysis, Springer, Berlin, 1977, p. 117.
[2] M. Henzler, in: I. Treusch (Ed.), Advances in Solid State Physics, vol. XIX, Vieweg, Braunschweig, 1979, p. 193.
[3] M. Henzler, Appl. Phys. A 34 (1984) 205.
[4] B. Müller, M. Henzler, Rev. Sci. Instrum. 66 (1995) 5232.
[5] M. Henzler, Surf. Sci. 298 (1993) 369.
[6] R. Feidenhans'l, Surf. Sci. Rep. 10 (1989) 105.
[7] I.K. Robinson, D.J. Tweet, Rep. Prog. Phys. 55 (1992) 599.
[8] J.M. van Hove, P. Pukite, P.I. Cohen, J. Vac. Sci. Technol. A 1 (1983) 609.
[9] G.E. Crook, K.G. Eyink, A.C. Campbell, D.R. Hinson, B.G. Streetman, J. Vac. Sci. Technol. A 7 (1989) 2549.
[10] B. Müller, Profilanalyse bei der Reflexionselektronenbeugung (RHEED): Elastische und Inelastische Streuung, VDI-Verlag, Düsseldorf, 1994.
[11] U. Scheithauer, G. Meyer, M. Henzler, Surf. Sci. 178 (1986) 441.
[12] M.G. Lagally, Diffraction Techniques, Academic Press, New York, 1985.
[13] P.K. Larsen, P.J. Dobsen, Reflection High-Energy Electron Diffraction and Reflection Electron Imaging of Surfaces, NATO ASI, vol. B 188, New York, 1987.
[14] M. Horn-von Hoegen, H. Pietsch, Surf. Sci. 321 (1994) L129.
[15] B. Voigtländer, A. Zinner, Surf. Sci. 292 (1993) L775.

[16] B. Voigtländer, A. Zinner, T. Weber, H.P. Bonzel, Phys. Rev. B 51 (1995) 7583.
[17] H. Busch, M. Henzler, Surf. Sci. 167 (1986) 534.
[18] J. Wollschläger, J. Falta, M. Henzler, Appl. Phys. A 50 (1990) 57.
[19] B. Müller, L. Nedelmann, B. Fischer, H. Brune, K. Kern, Phys. Rev. B 54 (1996) 17858.
[20] H. Nakahara, M. Ichikawa, Appl. Phys. Lett. 61 (1992) 1531.
[21] H. Pietsch, Universität Hannover, 1993.
[22] A. Ichimiya, H. Nakahara, Y. Tanaka, Thin Solid Films 281 (1996) 1.
[23] H. Nakahara, A. Ichimiya, Surf. Sci. 241 (1991) 124.
[24] O.L. Krivanek, Y. Tanishiro, K. Takayanagi, K. Yagi, Ultramicroscopy 11 (1983) 215.
[25] M. Henzler, Appl. Phys. 9 (1976) 11.